Alloy design of precipitation hardenable 1-12 type Nd-Fe-M (M=Ti, B) alloys

S.H. Huang , T.S. Chin and J.M. Yau

Department of Materials Science and Engineering Tsing Hua University,
Hsinchu, 300, TAIWAN, Republic of China

Typically two alloy systems were designed, i.e., the A-alloys: $(NdFe_{11}Ti)_{1-x}$-$(Nd_2B)_x$. and the B-alloys: $(NdFe_{11}Ti)_{1-y}$-$(Nd_2Fe_{14}B)_y$. Hard magnetic phase $Nd_2Fe_{14}B$ (2-14-1) had been expected and was successfully precipitated in the melt-spun $ThMn_{12}$ type (1-12) alloys by suitable heat treatment and coercivity was greatly enhenced. For the A-alloys, peak coercivity of 16.8 kOe was achieved at x= 0.4, while 11 kOe at x= 0.3 in which the 1-12 phase is the matrix with 17 vol% 2-14-1 precipitate phase. For the B-alloys, peak coercivity of 11 kOe was achievable at y= 0.7, in which the 2-14-1 and large amount of α-Fe coexist. By fitting coercivity vs. temperature curves with Guant's model, the coercivity mechanism of the above alloys can be attributed to arise from domain wall pinning of the 2-14-1 precipitate.

1. INTRODUCTION

In designing a precipitation hardenable alloy, magnetically hard phase(s), such as the $SmCo_5$, can be dispersed in the `softer' matrix, such as the $Sm_2(Co,Fe, Cu)_{17}$, by annealing (for precipitation or crystal-lization) or mechanical alloying to greatly enhance the coercivity of the softer matrix phase. In this study, the $Nd_2Fe_{14}B$ phase (2-14-1 for short) is chosen as (1) a crystallized phase in the melt-spun amorphous $NdFe_{11}Ti$-Nd_2B alloys[1] (A-alloys); or (2) a doping phase to the $NdFeTi_{11}$-Nd_2B alloy making up a pseudobinary system (B-alloys). Since there is no availabe phase relation between the 1-12 and the 2-14-1 phases, it is not clear whether there is solubility of the 2-14-1 phase in the 1-12 or vice verse. One straightforward choice is the trial to crystallize the two phases from the amorphous state, which is readily obtainable by melt-spinning technique, and suitable heat treatment.

In this report, detailed studies on magnetic properties, the TEM microstructure and the fitting of pinning models of the precipitation hardenable 1-12 type Nd-Fe-M (M= Ti, B) alloys are presented.

2. EXPERIMENTAL

The A-alloys: $(NdFe_{11}Ti)_{1-x}$-$(Nd_2B)_x$ and B-alloys: $(NdFe_{11}Ti)_{1-y}$-$(Nd_2Fe_{14}B)_y$ were prepared by arc-melting the constituent pure elements, and then melt-spinning onto a copper wheel at a constant substrate velocities of 30 m/s under Ar atmosphere. The spun ribbons were then heat-treated under different condition, as shown in Table 1. X-ray diffraction patterns (XRD) were directly obtained from the free surface of the ribbons with Cu-Kα radition. Magnetic properties were measured by a vibrating sample magneto-meter (VSM) with a maximum applied field of 2 T. The temperature dependence of iHc was obtained from hysteresis loops run at a series of fixed temperatures between 80 and 300 K using a SQUID magnetometer. Thermomagnetic behavior were examined with a thermomagnetic balance in an applied field of about 40 mT at a heating rate of 10 °C/min. Microstructural studies were made by using a JOEL model JEM 2000 FX scanning transmission electron microscope.

Table 1   The annealing routes for the alloys

I.D.	Heating Rate	Annealing Routes
H1	7 °C/min	800°C×60'→Water Quench(W.Q.)
H11	100 °C/min	800°C×60'→W.Q.
H12	7 °C/min	800°C×30'→W.Q.
H2	7 °C/min	700°C×60'→W.Q.
H3	7 °C/min	650°C×60'→W.Q.
H4	7 °C/min	630°C×60'→W.Q.
H5	7 °C/min	600°C×60'→W.Q.
P2	7 °C/min	650°C×10'→W.Q.→800°C×30'→W.Q.
P21	7 °C/min	650°C×10'→W.Q.→800°C×60'→W.Q.

3. RESULTS AND DISCUSSION

3.1. Magnetic properties of the studied alloys

The 30 m/s melt-spun alloys are amorphous as verified with XRD. In order to investigate the effect of the phase crystalized after different annealings, a series of annealing routes were designed, as shown in Table 1. For **P**-annealings, the soaking at 650 °C for only 10 minutes was designed to nucleate 2-14-1 nuclei in the amorphous matrix firstly (avoiding its growth), then rapidly heated to 800 °C and isothermal soaking there for various periods to nucleate the 1-12 phase and to grow both phases.

Figure 1 shows demagnetization curves of $(NdFe_{11}Ti)_{1-x}(Nd_2B)_x$ alloys after **H2** or **P** annealing. The maximum coercivity (iHc) of 16.8 kOe is achieved for the x= 0.40 alloy. A shoulder is visible for the x=0.25, 0.30 (**H2**) and x=0.4 (**P2**) alloys denoting the possible coexistence of a magnetically soft phase and a hard phase. This provides the first evidence that a magnetically hard phase exists to greatly enhance iHc. The iHc increases with increasing x values. For the x= 0.25 alloy, iHc can be improved from 200 Oe at the as-spun state to 4.2 kOe after the **H2** annealing. The coercivity of x= 0.4 alloy (10.5 kOe) after the **P2** annealing is lower than those after other annealings. These provide the second evidence that the annealed structure may play a very important role. The design is correct, as to be depicted in Sec. **3.2.** and Fig. 2.
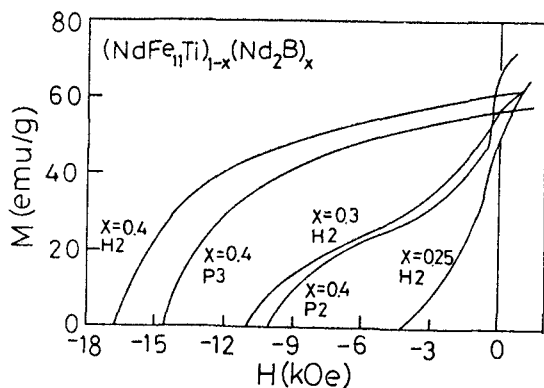
Table 2 shows magnetic properties of **H2** annealed **B**-alloys. Optimum properties of iHc=11.2 kOe, $4\pi Mr$= 9kG and $(BH)_m$= 12.5MGOe were obtained for the y= 0.7 $(Nd_{10.8}Fe_{82.9}B_{4.4}Ti_{1.9})$ alloy which has low level of Nd and B contents.

Table 2 Properties of **H2** annealed **B**-alloys

y=	0.2	0.4	0.5	0.6	0.7	0.8
iHc	0.5	1.0	4.8	8.2	11.2	7.1
$4\pi Mr$	88.8	79.0	83.6	80.0	92.8	81.2
$4\pi Ms$	148	131	129	119	124	135
Mr/Ms	0.60	0.61	0.65	0.67	0.75	0.60

*iHc in kOe, $4\pi Mr$ and $4\pi Ms$ are in emu/g

3.2. Thermomagnetic analyses and phase identification of annealed alloys

Curie temperatures (Tc) of the studied alloys vary greatly due to different annealing routes. There are two Tc's corresponding to the 1-12 and 2-14-1 phases after one-step **H1, H2, H3, H4** annealings for the A-alloys at x≤ 0.3 alloys. Tc's of the 1-12 and 2-14-1 phases are visvble for annealed x≤0.40 alloys after the two-step **P2** annealing. The XRD patterns of annealed A-alloys alloys after **P2** annealing, as shown in Fig. 2, also show free iron and 1-12 phases in all the A-alloys. This provides the evidence that 1-12 phase in highly Nd_2B-doped alloys after the **P2** annealing.

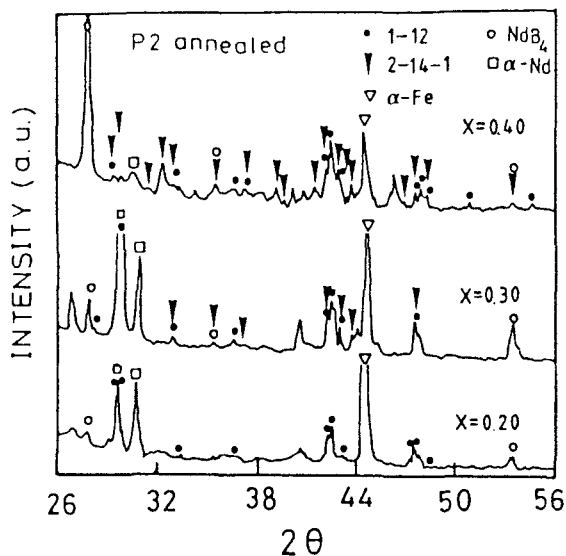Fig. 1 Demagnetization curves for the **H2**, **P2** or **P21** annealed A-alloys.

Fig. 2 XRD patterns for the A-alloys after **P2** annealing.

While after prolonged annealing at the same temperature (**P21**) free iron decreases and the 2-14-1 phase appears, free iron can not be found in the x≥ 0.3 alloys and the 1-12 phase disappears in the x≥ 0.35 alloys. The 2-14-1 phase becomes the major magnetic phase in the x= 0.4 alloy, in which no 1-12 nor free iron can be identified.

The XRD of the **H2** annealed **B**-alloys show that the reflection of free iron is much higher than those of the 2-14-1 phase, denoting a substantial amount of free iron. Thermomagnetic curves compared with those of $NdFe_{11}Ti$ and $Nd_2Fe_{14}B$ phases in the **B**-alloys are worked out. For y< 0.4 alloys, Tc of 1-12 phase (279°C) disappear, instead of transition phase around 180°C which belongs probably to an unknown Nd-Fe(Ti) phase appears[2]. For y≥ 0.4 alloys, Tc of 2-14-1 phase (around 310°C) appear and the 2-14-1 phase becomes dominating as y≥ 0.6. From the XRD and thermomagnetic studies, it is clear that the addition of the 2-14-1 composition into the $NdFe_{11}Ti$ results in the equilibrum phases of free iron and a Nd-Fe(Ti) for 0< y< 0.4, while free iron and the 2-14-1 for y≥ 0.5.

3.3. Temperature dependence of the coercive field

In Guant's model, the temperature dependence of coercivity is based on thermal activation over a random inhomogeneities [3]. Strong domain wall pinning will follow a thermal activation of the domain wall over pinning barriers given by

$$(iHc/H_0)^{1/2}=1-(75kT/4bf)^{2/3}, \qquad (1)$$

where k i2 Boltzmann's constant, b is the range of the pinning interaction and f is the maximum pinning force per pin. But the weak domain wall pinning implies a temperature dependence of coercivity given by

$$iHc/Ho=1-(25kT/2N_\gamma b^2), \qquad (2)$$

where γ is the wall energy per unit area. Hence, the plots showing temperature dependence of coercivity reflects the type of domain wall pinning.

Figure 3 respents the temperature dependence of coercive field of the **P2** annealed x= 0.25 **A**-alloy (a), the **H2** annealed **A**-alloys at x= 0.4 and **B**-alloys at y= 0.7 (b). There are two types of temperature dependence of iHc showing different domain wall pinnings. For **A**-alloys, the **P2** annealed x= 0.25 alloy, a linear relationship between iHc and T is a best fit at 160 to 300K,

denoting a weak pinning, as shown in Fig. 3(a). While for the **H2** annealed x≥0.4 alloys, a linear relationship between $iHc^{1/2}$ and $T^{2/3}$, appear at 180 to 320K, denoting a strong pinning, as shown in Fig. 3(b).

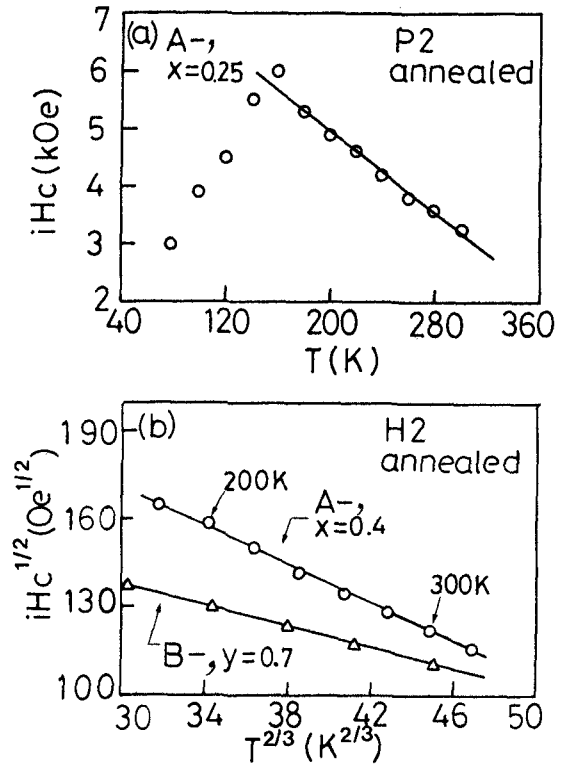Fig. 3 Temperature dependence of coercivity for the **P2**-annealed x= 0.25 alloy (a), and the **H2**-annealed x= 0.4 and y= 0.7 alloys (b).

The dependence of coercivity on temperature of annealed **B**-alloys reveal a linear relationship between $iHc^{1/2}$ and $T^{2/3}$, depicting a strong pinning, as shown in Fig. 3(b). From the fact that coercicity increases with increasing amount of the 2-14-1 phase for y≥ 0.5 alloys, it is evident that the 2-14-1 phase provides the strong pinning sites in the **B**-alloys.

The pinning mode obviously depends on the composition as well as heat treatment. It is thus very important to understand the microstructural features resulting from heat-treating different compositions.

3.4. Microstructural features

From TEM analyses [4], the 2-14-1 crystallites disperse around $Nd(Fe,Ti,B)_{12}$ grain boundaries or inside the $Nd(Fe,Ti,B)_{12}$ grain for annealed $x \leq 0.3$ A-alloys. They are sphere-like and discrete (island) in the 1-12 matrix ranging from 40 to 80 nm in diameter. Figure 4 shows the volume fraction, of the crystallized 2-14-1 phase and coercivity of the A-alloys after the **H1** annealing. It is manifest that the
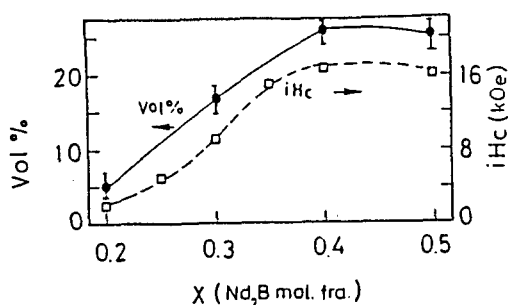

Fig. 4   Dependence on composition of the volume fraction and the coercivity of the crystallized 2-14-1 phase of the A-alloys after **H1** annealing.

coercivity can be correlated directly to the volume fraction of the crystallized 2-14-1 phase, not the grain size nor mean free path of the 2-14-1 phase. This provides a strong evidence of domain wall pinning by the crystallized 2-14-1 phase.

From TEM analyses of some of the **H2** annealed B-alloys, it is manifest that in addition to the 2-14-1 phase, a high density of free iron with a size around 60 nm can be oberved. The 2-14-1 grain size ranges from 30 to 80 nm, which is much smaller than the grain size of Nd-Fe-B sample made by the same presessing [5]. It is probably due to the grain refinement effect of the addition of Ti, whose presence is evidenced by energy dispersive x-ray spectra. The fine 2-14-1 grain thus contributes significantly to the coercivity by acting as an effective domain wall pinning site despite of the large amount of free iron.

4. CONCLUSIONS

Two series of precipitation hardenable Nd-Fe-M (M= Ti, B) alloys, i.e., $(NdFe_{11}Ti)_{1-x}-(Nd_2B)_x$ (the A-alloys) and $(NdFe_{11}Ti)_{1-y}-(Nd_2Fe_{14}B)_y$ (the B-alloys) have been worked out.

For A-alloys, peak coercivity of 16.8 kOe was achieved at x= 0.4, while 11 kOe at x= 0.3 in which the 1-12 phase is the matrix with 17 vol.% of 2-14-1 as the crystallized phase. The 2-14-1 phase becomes the major magnetic phase in the $x \geq 0.35$, alloys, in which 2-14-1 phase amounts to 20 vol.%. The coercive field increases in the same way as increasing volume fraction of the crystallized 2-14-1 phase, not the size nor mean free path. For **B**-alloys, the 1-12 phase is stable up to only y= 0.1; the 2-14-1 phase is stable as $y \geq 0.4$, and become major phase as $y \geq 0.6$. Peak coercivity of 11 kOe was obtained from **H2** annealed y=0.7 alloy with low level Nd and B contents.

By fitting coercivity vs. temperature curves with Gaunt's model, the coercivity mechanism of the above alloys can be attributed to arise from domain wall pinning of the 2-14-1 precipates, strong pinning or weak pinning prevails depending on composition and heat treatment.

REFERENCES

1. Z.R. Zhao, Y.G. Ren, K.D. Aylesworth, and D.J. Sellmyer, J. Appl. Phys., 63 (1988) 3699.
2. H.H. Stadelmaier, G. Schneider, E.-Th. Henig and M. Ellner, Mater. Lett., 10 (1991) 303.
3. P. Gaunt, Phil. Mag., B48 (1983) 261.
4. S.H. Huang, T.S. Chin, J. Appl. Phys., 70 (8), (1991) 4439.
5. R.K. Mishira, J. Magn. Magn. Mater., 54-57 (1986) 405.